

Unlocking potential: A case study on reducing shortwave radiation bias in the Southern Ocean through improved cloud phase retrievals based on machine learning

W. Schimmel^{1,2}, C. Barrientos-Velasco², J. Witthuhn^{1,2}, M. Radenz², B. Barja González³, and H. Kalesse-Los¹

¹Leipzig Institute for Meteorology, Leipzig University, Leipzig, Germany

²Leibniz Institute for Tropospheric Research (TROPOS), Leipzig, Germany

³Atmospheric Research Laboratory, University of Magallanes, Punta Arenas, Chile

Key Points:

- A Southern Ocean radiative closure study shows the potential of reducing short-wave radiation bias using a novel machine-learning cloud liquid retrieval.

Abstract

This study outlines the potential of machine-learning-augmented active remote sensing techniques for an accurate representation of the radiative effect of mixed-phase clouds. We utilize a combination of the machine-learning-based liquid-layer detection method VOODOO and a single-column radiative transfer model to evaluate downwelling short wave fluxes of a Southern-Ocean mixed-phase cloud case against ground-based pyranometer observations. A comparison against a standard radar-lidar processing chain reveals that the new approach provides insights into deep mixed-phase clouds, which were previously inaccessible using traditional lidar-based liquid-detection techniques. Specifically, VOODOO creates more realistic liquid water content distributions which significantly influence the profile of heating rates. Moreover, an improved estimation of shortwave cloud radiative effects of the VOODOO-based liquid identification in comparison to the conventional method was derived. The mean absolute error of simulated shortwave radiation at the surface was reduced by 70% from 44% for the conventional method to 8% for the VOODOO approach.

Plain Language Summary

This article discusses the challenges associated with accurately identifying liquid water layers within mixed-phase clouds, which is an important factor in understanding precipitation formation and for estimating cloud radiative effects. While remote-sensing retrievals using lidar can be useful for this purpose, they face limitations in optically thick or multilayer clouds, leading to biases in simulated radiative fluxes. To address this issue, the authors propose a machine-learning-based method called VOODOO designed to better detect supercooled-liquid in clouds. This methodology has the potential to reduce biases in radiative transfer simulations and improve model validation. A proof-of-concept study was conducted using a single-column radiative transfer calculation. This study compares the shortwave cloud radiative effects of mixed-phase clouds detected by Cloudnet algorithm and VOODOO to ground-based observations. The results demonstrate a reduction in shortwave radiation bias, suggesting that liquid-layer detection with machine-learning retrievals has the potential to improve radiative transfer simulations.

1 Introduction

In the Southern Ocean, supercooled liquid water clouds and mixed-phase clouds (MPC) are a prevalent atmospheric features (Hu et al., 2010; Kanitz et al., 2011; Morrison et al., 2011; Huang et al., 2012; Radenz et al., 2021). However, the region suffers from a scarcity of detailed long-term observations, particularly in the southern mid-latitudes. Existing observations are primarily based on limited-sensitivity instruments like lidar-only (Kanitz et al., 2011), space-borne radar-lidar (Zhang et al., 2010; Wang et al., 2016), or short-term ship-based measurements (Gettelman et al., 2020; Mace et al., 2021; Xi et al., 2022). The gap in long-term ground-based remote sensing of the atmosphere motivated the 3-year Dynamics, Aerosol, Clouds, And Precipitation Observations in the Pristine Environment of the Southern Ocean (DACAPO-PESO) field campaign in Punta Arenas (53.1°S, 70.9°W), Chile, and has already provided valuable insights, particularly into shallow mixed-phase clouds (Radenz et al., 2021).

Despite ongoing efforts, significant uncertainties in mixed-phase cloud representation persist in GCMs (McCoy et al., 2016). The correct representation of variables like cloud cover, cloud albedo, outgoing terrestrial radiation, and cloud water content is heavily influenced by the modeled temperature range of coexisting liquid water and ice, as highlighted by Li and Treut (1992) and Gregory and Morris (1996). Various GCMs predict widely differing thermodynamic cloud phase distributions at given temperatures, often failing to match observed spatial distributions and magnitudes (Bony et al., 2006;

Grise & Polvani, 2014a; Grise et al., 2015). Additionally, relying solely on vertically integrated water contents for GCM validation can exaggerate discrepancies in cloud radiative feedback, as suggested by Komurcu et al. (2014).

In the Southern Ocean, GCM estimates of cloud properties are notably uncertain. Common issues include underestimating the amount of supercooled liquid water in clouds, leading to biases in shortwave (SW) radiative fluxes (Kay et al., 2016; Bodas-Salcedo et al., 2016; Gettelman et al., 2020). Inaccuracies in cloud phase representation in reanalysis products (Naud et al., 2014) also contribute to the models' inability to accurately represent supercooled water frequencies in mixed-phase clouds. Even with correct total condensed water content estimations, the reduced albedo of ice-phase clouds due to fewer but larger ice particles compared to smaller and more numerous liquid droplets results in a lower optical thickness for glaciated clouds. Hence, accurately identifying the spatial distribution of liquid droplets in mixed-phase clouds is crucial, not only for their differing radiative properties (Sun & Shine, 1994) but also for their impact on precipitation formation (Field & Heymsfield, 2015; Mülmenstädt et al., 2015), affecting cloud lifetime.

The advancement of synergistic remote-sensing observations and the development of microphysical cloud property retrievals, such as cloud thermodynamic phase, significantly enhance our understanding of mixed-phase cloud processes (Shupe et al., 2005; Bühl et al., 2016; Mace & Protat, 2018; Griesche et al., 2020; Zaremba et al., 2020). Precise cloud thermodynamic phase retrievals are essential for refining GCM cloud phase representations (Fiddes et al., 2022). Studies indicate that shortwave radiative transfer, particularly through mixed-phase clouds, is highly dependent on the quantity and location of liquid cloud droplets (McFarquhar et al., 2021; Barrientos-Velasco et al., 2022). An underestimation of liquid water path (LWP) results in less opaque clouds, leading to an underestimated shortwave cloud radiative effect at the surface (Cesana & Storelvmo, 2017; Tan & Storelvmo, 2019).

In this study, we explore the potential of the enhanced cloud phase retrieval method named Cloudnet-VOODOO, to mitigate the SW radiation bias observed in the Southern Ocean. Our analysis is anchored on a single case study from January 2, 2019, in Punta Arenas, Chile, conducted during the DACAPO-PESO field campaign. This case study not only provides specific insights but also serves as a proof-of-concept for subsequent, more extensive investigations. The findings and methodologies applied here lay the groundwork for future research, potentially leading to broader applications and deeper understanding in the field.

The structure of this work is organized as follows: Section 2 introduces the dataset, followed by Section 3, which describes of the enhanced cloud phase detection algorithm VODOO. This section also details the set-up of the radiative transfer simulation employed in our study. In Section 4, we present the outcomes of our study, focusing on the evaluation of our method's effectiveness in addressing the SW radiation bias. Conclusions and an outlook are given in Section 5.

2 Datasets

2.1 Primary data sources

The core instrumentation used for this work is provided by the Leipzig Institute for Meteorology (LIM) and the Leibniz Institute for Tropospheric Research (TROPOS). The study utilizes five distinct data sources, enumerated as below. Additional information about the instruments is provided in Table 1.

1. Profiles of cloud radar Doppler spectra and moments, sourced from the RPG-FMCW94-DP, which is a 94 GHz frequency-modulated continuous-wave (FMCW), vertically-pointing Doppler cloud radar with polarimetric capabilities.
2. Attenuated backscatter coefficient (β_{att}) profiles, obtained from the Jenoptik CHM15kx, a ceilometer operating at 1064 nm wavelength.
3. Liquid Water Path (LWP) measurements, retrieved from the RPG-HATPRO-G2. This instrument is a 14-channel microwave radiometer (MWR).
4. Atmospheric data including temperature, relative humidity, and pressure, collected from the European Centre for Medium-Range Weather Forecasts Integrated Forecasting System (ECMWF-IFS).
5. Shortwave downward irradiance data, as measured by a Class A pyranometer (ISO 9060:2018 standard), specifically the MS-80 model from EKO Instruments.

Table 1. Specifications of instruments/models and measured/modeled quantities used in this study.

| Data source (Reference) | Frequency ν Wavelength λ | Measured / retrieved quantity | Temporal resolution | Vertical range | Vertical resolution |
|--|---|---|------------------------|-------------------|------------------------|
| Doppler cloud radar RPG-FMCW-94-DP (Küchler et al., 2017) | $\nu = 94 \text{ GHz}$ | Spectral power $S(v_D)$ Radar reflectivity factor Z_e Mean Doppler velocity \bar{v}_D Spectrum width σ_w Linear depolarization ratio LDR | 5 s | 120–12000 m | 30–45 m |
| Microwave radiometer RPG-HATPRO-G2 (Rose et al., 2005) | $\nu = 22.24\text{--}31.4 \text{ GHz}$ $\nu = 51.0\text{--}58.0 \text{ GHz}$ | Brightness temperatures Liquid water path LWP | 1 s | column integral | |
| Ceilometer Jenoptik CHM15kx (Heese et al., 2010) | $\lambda = 1064 \text{ nm}$ | Attenuated backscatter coefficient β_{att} | 30 s | 15–15000 m | 15 m |
| Weather model forecast ECMWF-IFS ("ECMWF Forecast User Guide", 2018) | | Temperature T Pressure P Relative Humidity H | 3600 s | 10–12000 m | 20–300 m |
| Radiation MORDOR (<i>Mobile Radiation Observatory (MORDOR)</i> , 2022) | $\lambda = 0.3\text{--}4 \mu\text{m}$ | Shortwave downward irradiance SW | 1 s | column integral | |

The dataset of atmospheric state variables used as input parameters for the radiative transfer simulations are based on the hourly pressure level profiles of temperature, pressure, ozone mass mixing ratio and specific humidity from the European Centre for Medium-Range Weather Forecasts (ECMWF) Re-Analysis (ERA5), and single levels of surface pressure and skin temperature (Hersbach et al., 2020). The ERA5 dataset has a spatial grid from 0.25° latitude by 0.25° longitude. We opted for this dataset due its consistency and realistic representation of the atmospheric conditions as described in previous studies (Goyal et al., 2021; Hoffmann & Spang, 2022).

Although, the DACAPO-PESO field campaign was conducted over a period of three years (November 2018 – November 2021) we here focus on a single case study from January 2, 2019. This can be explained by three factors: Firstly, the RPG Doppler cloud radar which is the main instrument required for the novel thermodynamic phase retrieval, was only deployed for the first 9 months of the field campaign (November 2018 – September 2019). Secondly, high-quality surface pyranometer data crucial for validating the short-wave radiative transfer simulations was reliably obtained for only a continuous two-month period (January 2019 – February 2019). Thirdly, to conduct the presented analysis, several meteorological conditions have to be fulfilled. Those include a homogeneous cover of non-precipitating multilayer mixed-phase clouds during daylight. Given these constraints, only one case study could be identified during January 2019 – February 2019. This specific case study serves as an illustrative proof-of-concept study.

3 Methodology

The following section firstly describes the methods to retrieve the cloud macro- and microphysical properties used to generate the input data for the radiative transfer simulations (RTS). Secondly, it describes RTS framework used to model the shortwave irradiances and to derive the cloud radiative effects.

3.1 Description of Cloudnet and VOODOO

Cloud macro- and microphysical products like cloud base- and top height, liquid- and ice water content as well as effective radii of liquid droplets and ice particles are derived on a profile-by-profile basis from the presented ground-based data of MWR, cloud radar and ceilometer as well as temperature and pressure from the ECMWF-IFS (see Table 1). These products are essential as they form key input parameters for the radiative transfer simulations, were processed using the Cloudnet approach, additionally generates an atmospheric target classification, which categorizes each pixel in the spatio-temporal domain to a certain hydrometeor class (i.e. ice, cloud droplets, melting ice, drizzle, rain). We have adopted the processing chain of the classical multi-sensor methodology Cloudnet, originally conceptualized by Illingworth et al. (2007) by improving the liquid cloud droplet detection beyond lidar attenuation using Schimmel et al. (2022).

However, in Cloudnet the identification of liquid droplets relies entirely on the attenuated backscatter coefficient β_{att} of the lidar, which is quickly attenuated by liquid layers. For this reason, the liquid droplet detection of CloudnetPy beyond full lidar attenuation is not reliable, limiting the application to thin, single layer stratiform clouds. The new machine learning approach by Schimmel et al. (2022) is used as add-on to CloudnetPy, for revealing supercooled liquid layers beyond lidar attenuation (VOODOO). The VOODOO algorithm is based on a convolutional neural network. Radar Doppler spectra features are processed into a likelihood for the presence of liquid cloud droplets. Liquid cloud droplet predictions by VOODOO are used to augment the Cloudnet atmospheric target classification in altitudes where no valid lidar signal is received. Clearly, Cloudnet’s lidar-based approach has an advantage in detecting even thin liquid water layers, whereas VOODOO’s radar approach can be used primarily to reveal liquid water layers beyond lidar attenuation in multi-layer situations or deep mixed-phase clouds. Both approaches complement each other perfectly and are now available as Cloudnet target classification product in the latest Python-based GitHub release github.com/actris-cloudnet/cloudnetpy. The VOODOO method is also available as stand-alone version github.com/actris-cloudnet/voodooonet.

In addition, Cloudnet provides the derivation of microphysical products, such as Ice Water Content (IWC) and Liquid Water Content (LWC), as well as effective radii of ice crystals ($r_{\text{eff}}^{\text{ice}}$) using Hogan et al. (2006); Delanoë et al. (2007); Griesche et al. (2020); Frisch et al. (2000) and liquid droplets ($r_{\text{eff}}^{\text{liq}}$) using Frisch et al. (1995, 1998, 2000). The implementation of the Cloudnet algorithm is based on its latest iteration, CloudnetPy, which is described in detail in Tukiainen et al. (2020). Crucially, for the purposes of this study, all Cloudnet-derived products have been systematically regridded to a uniform grid using the radar range resolution and a temporal resolution of 30 seconds.

3.2 Description of T-CARS

The radiative transfer simulations were carried out using the TROPOS – Cloud and Aerosol Radiative effect Simulator (hereafter T-CARS). T-CARS is a Python-based environment created to conduct radiative transfer simulations with a particular focus on the investigation of the radiative effects of aerosols, and clouds (Barlakas et al., 2020; Witthuhn et al., 2021; Barrientos-Velasco et al., 2022). The radiative transfer solver used is a 1D single column rapid radiative transfer model (RRTM) for GCM applications (RRTMG;

Mlawer et al. (1997); Barker et al. (2003); Clough et al. (2005)). T-CARS output files have a standard atmospheric grid that consists of 197 levels ranging from the surface up to 20 km height at 1-minute temporal resolution, as described in Barrientos-Velasco et al. (2022) and published on Zenodo (Barrientos-Velasco, 2023). The first 10 km of the atmosphere is divided into 160 levels with a geometric layer thickness of about 62.5 m. The level thickness of each pixel for the first 10 km of the atmosphere corresponds to two vertical levels of Cloudnet pixels, which are averaged to the standard grid. This configuration ensures that the atmospheric grid does not exceed the model set-up limit of 200 atmospheric levels. The T-CARS output files provide simulated clear-sky and all-sky atmospheric profiles of broadband longwave (LW) and SW radiative fluxes and heating rates. We focus on the SW broadband flux by calculating the flux difference between simulated and observed radiative fluxes, describing heating rates and computing the SW cloud radiative effect (CRE) following Eq. 1.

$$CRE_{SW,BOA} = (F_{SW}^{\downarrow} - F_{SW}^{\uparrow})_{All-sky} - (F_{SW}^{\downarrow} - F_{SW}^{\uparrow})_{Clear-sky}. \quad (1)$$

4 Results

The results are divided into two subsections. The first subsection offers a detailed overview of the cloud conditions on January 2, 2019, in Punta Arenas, Chile. This is followed by the description of the cloud microphysical quantities retrieved using Cloudnet and the enhanced retrieval method, VOODOO. The second subsection focuses on the analysis of the radiative transfer simulations, contrasting simulations using solely Cloudnet (termed Cloudnet-Sim or CSim) with those combining VOODOO and Cloudnet inputs (referred to as VOODOO-Cloudnet-Sim or VCSim). This section focuses on evaluating the bottom-of-atmosphere (BOA) downwelling shortwave (SWD) radiative fluxes and includes calculations of the shortwave cloud radiative effect (CRE) and the SW heating rate. The distinctions and insights derived from these simulations are presented in Table 2, Fig. 3, and Fig. 4, offering a nuanced view of the methodologies' impact.

4.1 Cloud microphysical retrieval results

In the first step of this analysis, we quantify the effects of the improved thermodynamic phase classification by VOODOO in comparison to the reference retrieval, Cloudnet.

We focus on the period between 15:00–22:00 UTC on 2 January 2019 in Punta Arenas Chile, when multilayer mixed-phase clouds were observed. Figure 1 shows the radar reflectivity factor Z_e (A), the target classification of Cloudnet (B) and the combined target classification of Cloudnet+VOODOO (C). During the first half of the case study, multiple showers of low precipitation intensity were observed by the radar. However, no measurable precipitation reached the ground-based in-situ rain sensors. The ceilometer cloud base height shown by red dots in Fig. 1 (A) indicates the supercooled liquid layer heights, that match the liquid detection (classes: 'Droplets' and 'Ice & droplets') in the Cloudnet target classification (B). However, as described above, the lidar-based liquid detection in the standard Cloudnet algorithm is only possible until full lidar attenuation, thus liquid layers at higher altitudes remain undetected. In contrast, VOODOO reveals additional supercooled liquid layers in altitudes between 2.5–5.0 km with cloud top temperatures down to $T = -25^\circ \text{C}$.

The enhanced liquid detection of VOODOO is used in the next step to improve the Cloudnet products, which are required input parameters for the radiative transfer simulations, namely IWC and LWC as shown in Fig. 2 and effective radii of ice crystals and droplets (not shown). The IWC values, as shown in panel (A), are consistent between Cloudnet and VOODOO, ranging from 10^{-5} to $2 \times 10^{-4} \text{ kg m}^{-3}$. This is because both

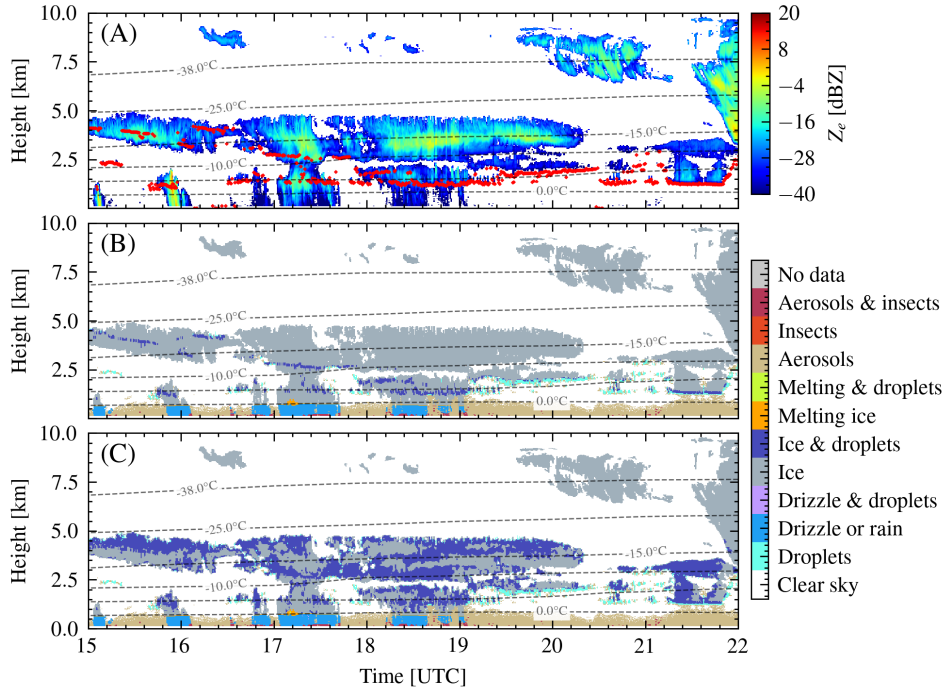


Figure 1. Cloud situation on 2 January 2019 in Punta Arenas, Chile. (A) Radar reflectivity Z_e , (B) atmospheric target classification of Cloudnet, and (C) combination of atmospheric target classification of Cloudnet enhanced by the liquid predictions of VOODOO. Dashed lines depict the isotherm lines from ECMWF temperature profiles. The red dots in (A) indicate the ceilometer cloud base height.

Cloudnet and VOODOO utilize all ice-containing classes (such as 'ice' and 'ice + droplets') from the target classification to compute the IWC. However, differences in the distribution of the liquid layers within the observed clouds are clearly visible in Fig. 2 (B), (C). The scaling approach used in Cloudnet, distributes all liquid water detected by the MWR into the thin liquid layers (with depths < 150 m), resulting in Cloudnet mean LWC values of $3 \times 10^{-3} \text{ kg m}^{-3}$. In contrast, the use of VOODOO for liquid detection enables the LWC to be distributed over a broader depth of liquid layers, resulting in reduced average LWC values per volume of $5 \times 10^{-4} \text{ kg m}^{-3}$.

4.2 Analysis of simulated SW radiative fluxes and heating rates

Single column radiative transfer simulations were conducted to quantify the SW radiative effect of varying cloud microphysical properties, based on Cloudnet (CSim) and VOODOO (VCSim). This analysis primarily focused on comparing irradiances and cloud radiative effects of SWD simulations using T-CARS to SWD observations at BOA, as depicted in Figure 3 A and B, and atmospheric SW heating rates shown in Figure 4. The findings are summarized in Table 2.

The comparison distinguishes between periods of homogeneous and inhomogeneous cloud cover, with the latter indicated by grey patches in Figure 3 starting at 20:00 UTC and 21:00 UTC. This differentiation is crucial when comparing pencil-beam radar-lidar observations against the hemispherical view of the broadband pyranometer measurements. It is important to note that conditions with broken clouds starting at 15:00 UTC and 16:20 UTC were excluded from the comparison. Under these broken cloud conditions,

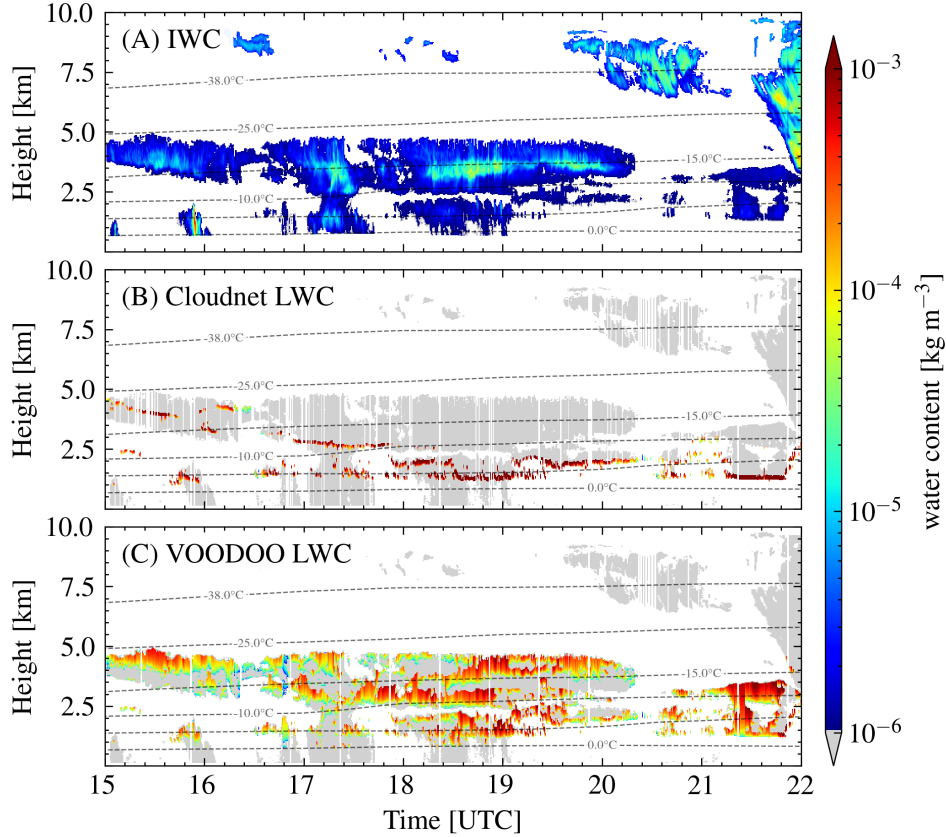


Figure 2. Panel (A) shows ice water content derived from both, Cloudnet and VODOO, for 2 January 2019 in Punta Arenas, Chile. (B) Cloudnet liquid water content, and (C) Cloudnet liquid water content enhanced by liquid predictions of VODOO. In (B) and (C), colored pixels reflect liquid-bearing cloud volumes and grey pixels other hydrometeor types (see Fig. 1). Dashed lines depict the isotherm lines from ECMWF temperature profiles. The corresponding liquid water path to panel B and C is shown in Fig. 3A.

multiple scattering of SW radiation increases the diffuse SW, leading to larger values than those observed during clear-sky conditions, which complicates the comparison with the simulations.

The comparative analysis between simulated and observed SWD fluxes at BOA (Figure 3 A) reveals a closer agreement between the simulations and pyranometer observations when incorporating VODOO-based inputs compared to Cloudnet-only inputs. VCSim demonstrates a significant reduction in the mean absolute bias of SWD radiation by 70 % under homogeneous cloud conditions. While reductions are also observed during broken cloud conditions in VCSim, they are comparatively less pronounced. However, it is important to acknowledge that one-dimensional radiative transfer simulations are less effective in resolving broken cloud conditions. More sophisticated methodologies such as three-dimensional radiative transfer models would be required to accurately capture such conditions. This type of analysis is not within the scope of this study.

Panel B in Figure 3 displays the time series of the calculated $CRE_{SW,BOA}$ using CSim and VCSim, alongside a computation that substitutes simulated all-sky SWD flux with downwelling pyranometer observations. The results show a strong agreement be-

Table 2. Table of BOA-SWD radiation fluxes and $CRE_{SW,BOA}$. Shown are time-series mean values (Mean) in $W m^{-2}$, correlation coefficient (r^2), root mean squared error (RMSE) in $W m^{-2}$, mean absolute error (MAE) in $W m^{-2}$, of pyranometer (Obs) as well as T-CARS simulations using Cloudnet (CSim) or VOODOO-Cloudnet (VCSim) as input for the case study on 2 January 2019 in Punta Arenas, Chile. Results cover two scenarios: 'inhom', analyzing the entire 15:00 to 22:00 UTC period, and 'hom', focusing on homogeneously distributed stratiform clouds without broken cloud effects.

| | | Mean | r^2 | RMSE | MAE |
|----------------|--------|--------------------|--------------|--------------|--------------|
| | | Obs / CSim / VCSim | CSim / VCSim | CSim / VCSim | CSim / VCSim |
| BOA-SWD | inhom. | 274 / 564 / 349 | 0.53 / 0.73 | 381 / 180 | 315 / 125 |
| | hom. | 191 / 432 / 234 | 0.50 / 0.77 | 345 / 126 | 251 / 74 |
| $CRE_{SW,BOA}$ | inhom. | -511 / -247 / -437 | 0.42 / 0.70 | 348 / 177 | 290 / 124 |
| | hom. | -499 / -281 / -457 | 0.32 / 0.79 | 313 / 126 | 229 / 74 |

tween VCSim (red dots) and calculations using observational data (blue line), resulting in correlation coefficients above 0.7 in both homogeneous and when including inhomogeneous cloud conditions. Due to the underestimation of supercooled liquid occurrence higher up in the atmospheric column, CSim-based simulations lead to a strong underestimation of SW cooling at BOA (Fig. 3B, black dots). Because of the improved supercooled-liquid detection, VCSim results of $CRE_{SW,BOA}$ qualitatively match the pyranometer-based CRE better and lead to a reduction in the mean absolute error by 68 % compared to CSim results. The mean percentage error of $CRE_{SW,BOA}$ between CSim and pyranometer observations is 44 %, while VCSim reduces this error to 8 % for homogeneous cloud conditions, as detailed in Table 2.

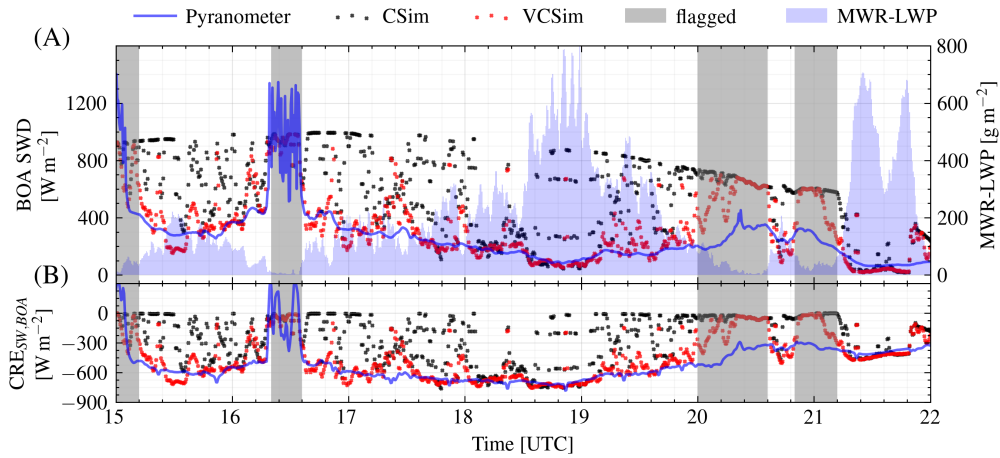


Figure 3.

(A) Time series of bottom-of-atmosphere (BOA) shortwave downwelling irradiance pyranometer observations (blue line, left y-axis), simulations (black and red dots, left y-axis) and retrieved MWR-LWP (blue bars, right y-axis). (B) Time series of BOA cloud radiative effect based on simulated SW fluxes for Cloudnet (black dots) and VOODOO+Cloudnet (red dots). Boxes flagged in gray indicate time frames with broken clouds or inhomogeneously distributed clouds.

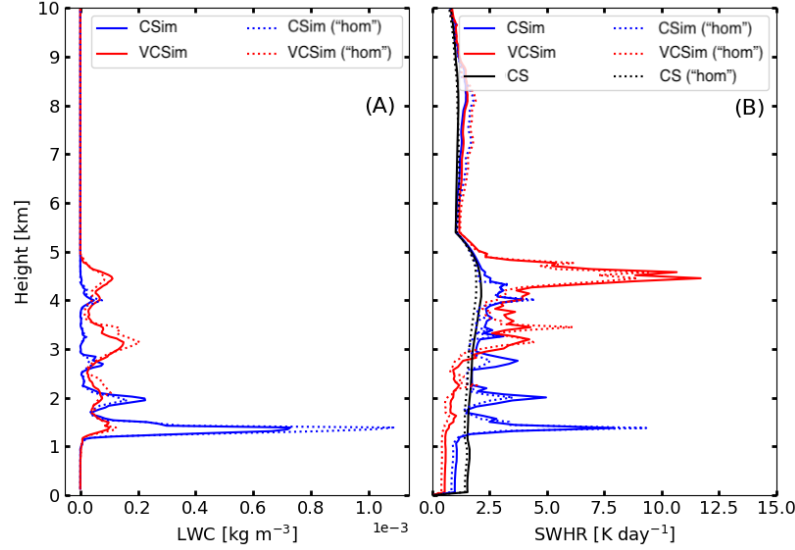


Figure 4. Mean profiles of liquid water content (LWC) in (A) and shortwave atmospheric heating rate (SWHR) for all-sky conditions for Cloudnet (blue line), VODODO-Cloudnet (red line), and clear-sky (CS; black line) in panel (B). Solid lines show SWHR for the entire period 15:00–22:00 UTC on 2 January 2019 and dotted line for homogeneous clouds ("hom") only.

The calculation of the atmospheric change in the net SW flux (i.e., downwelling SW minus upwelling SW flux) in the atmosphere is expressed in terms of SW heating rates. Atmospheric heating rates quantify the cloud-induced changes in the temperature profile in the vicinity of clouds. We computed the SW heating rates (SWHR) for both VCSim and CSim results. This analysis highlights the impact of liquid layer locations on the SW heating effect, as depicted in Figure 4.

Notably, the VCSim simulations, which retrieve liquid layers up to approximately 4.5 km height, result in significant cloud top warming of up to 12 K per day. This warming effect at higher altitudes concurrently mitigates warming in the lower atmosphere due to a portion of this radiation being reflected upward. In contrast, CSim-based simulations, which predominantly feature cloud opacity around 1.5 km, yield a SWHR of approximately 9 K per day at this height.

Overall, the mean SWHR remains relatively consistent between homogeneous and inhomogeneous cloud conditions. The minor variations observed in Figure 4B primarily stem from an increase in LWC under homogeneous cloud conditions, as elaborated in Figure 4A. Additionally, it's noteworthy that the clear-sky profiles, represented by a solid black line in Figure 4B, exhibit marginally positive SWHR due to increased water vapor at cloud heights.

5 Discussions, Conclusions and Outlook

This study demonstrates the integration of radiative transfer models with the innovative machine learning method, VODODO, for cloud liquid detection. Our findings illustrate a reduction in shortwave (SW) radiation biases and enhancements in estimates of SW heating rates. The study focuses on a multilayer mixed-phase cloud case study in the Southern Hemisphere in Punta Arenas, Chile. The approach consists in improving the multi-sensor products (LWC and $r_{\text{eff}}^{\text{liq}}$) of Cloudnet by using VODODO. Single

column 1D radiative transfer simulations were conducted to assess the applicability of VOODOO and Cloudnet and quantify the differences in radiative fluxes at BOA. Given the availability of ground-based radiation flux measurements, our analysis focused on the broadband SW fluxes. The key findings are summarized below:

- VOODOO-based simulations exhibit a significant reduction in SW flux biases at BOA of more than 70 % (MAE) and 63 % (RMSE), suggesting a great improvement to the use of the Cloudnet retrievals alone.
- Regarding CRE_{SW} at BOA, our results improved the liquid detection of VOODOO leads to a significant reduction in SW radiation bias of CRE of 67 % (MAE) and 60 % (RMSE) in multi-layer cloud situations compared to the Cloudnet-only microphysical retrievals.
- The value of observed CRE_{SW} of about -500 W m^{-2} for the presented multilayer mixed-phase cloud is consistent with the findings of Protat et al. (2017), who report values of CRE_{SW} of up to -440 W m^{-2} for March 2015 in the Southern Ocean, and with Grise and Polvani (2014b) indicating significant CRE_{SW} ranging from -120 to -150 W m^{-2} for the location of Punta Arenas during summer based on satellite observations and model evaluations. It is important to note, however, that their results are averaged for a more extended period and area of analysis, thus the magnitude of the values is lower. The large instantaneous CRE_{SW} values presented in our study are predominantly influenced by the presence of supercooled liquid layers in mixed-phase clouds characteristic of the region, as discussed in Bodas-Salcedo et al. (2016).
- The comparison of SWHR revealed a significant difference in the altitude of the SW warming effect. This underscores the importance of accurately retrieving the distribution of liquid water content within clouds, as it has a profound effect on radiation. This effect is particularly pronounced in stratiform clouds, where atmospheric radiation plays a more significant role in the diabatic heating of the atmosphere. This, in turn, can potentially perturb the local atmospheric stability (Turner et al., 2018).

The presented proof-of-concept study outlines the promising application of VOODOO to reduce shortwave radiation biases caused by the misclassification of cloud thermodynamic phase and the subsequent inaccuracies in locating LWC within the atmospheric column, which is crucial for Southern Ocean clouds. This technique holds potential for addressing similar challenges in other regions where MPC representation is challenging, as previously described (Barrientos-Velasco et al., 2022; Fiddes et al., 2022).

However, it is important to note that the current analysis has limitations. The Doppler spectrum-based liquid detection VOODOO was originally designed for cloud radars of type RPG-FMCW and has yet to be adapted for use with cloud radars from other manufacturers. This would allow for analysis of other Southern Ocean field campaign data such as ARM MARCUS campaign (Xi et al., 2022).

Future studies should also be extended to consider the effect of longwave radiative flux. Moreover, there is a plan to test the VOODOO-based method on future long-term Southern Ocean deployments of the Leipzig Aerosol and Cloud Remote Observations System (LACROS) station on the South Island of New Zealand. These efforts aim to enhance the understanding of cloud-radiation interaction field campaigns in this critical region planned for 2025-2026.

Acknowledgments

This research was supported by the Federal State of Saxony and the European Social Fund (ESF) in the framework of the programme “Projects in the fields of higher ed-

ucation and research” (grant no. 100339509) and ESF-REACT (grant no. 100602743). We gratefully acknowledge the Bundesministerium für Bildung und Forschung for the project “Combining MOSAiC and Satellite Observations for Radiative Closure and Climate Implications” (MOSaRiCs) – Project Number 03F0890A. Additionally, we acknowledge the National Fund for Scientific and Technological Development of Chile, FONDECYT, through grant agreement No. 11181335. We gratefully acknowledge the funding of the German Research Foundation (DFG) in the frame of the special priority program on the Fusion of Radar Polarimetry and Atmospheric Modelling (SPP-2115, PROM, Grant KA 4162/2-1) and the European Union (EU) Horizon 2020 project (ACTRIS; grant no. 654109).

6 Code and Data Availability Statement

The CloudnetPy framework, incorporating the VOODOO processing, is accessible at the CloudnetPy GitHub Repository <https://github.com/actris-cloudnet/cloudnetpy>. Additionally, a stand-alone version of VOODOO can be found at <https://github.com/actris-cloudnet/voodooonet>. For the Cloudnet products and the data files enhanced by VOODOO, please refer to the Zenodo Cloudnet and VOODOO Dataset <https://doi.org/10.5281/zenodo.7760395>. The data files generated from the radiative transfer simulations in this study are also available on Zenodo via <https://doi.org/10.5281/zenodo.7674862>.

References

- Barker, H. W., Stephens, G. L., Partain, P. T., Bergman, J. W., Bonnel, B., Campana, K., ... Yang, F. (2003). Assessing 1d atmospheric solar radiative transfer models: Interpretation and handling of unresolved clouds. *Journal of Climate*, 16(16), 2676 - 2699. Retrieved from https://journals.ametsoc.org/view/journals/clim/16/16/1520-0442_2003_016_2676_adasrt_2.0.co_2.xml doi: 10.1175/1520-0442(2003)016<2676:ADASRT>2.0.CO;2
- Barlakas, V., Deneke, H., & Macke, A. (2020). The sub-adiabatic model as a concept for evaluating the representation and radiative effects of low-level clouds in a high-resolution atmospheric model. *Atmospheric Chemistry and Physics*, 20(1), 303–322. Retrieved from <https://acp.copernicus.org/articles/20/303/2020/> doi: 10.5194/acp-20-303-2020
- Barrientos-Velasco, C. (2023, March). *Single column 1D radiative transfer simulations for a case study of low-level-stratus clouds in the central Arctic during PS106*. Zenodo. Retrieved from <https://doi.org/10.5281/zenodo.7674862> doi: 10.5281/zenodo.7674862
- Barrientos-Velasco, C., Deneke, H., Hünerbein, A., Griesche, H. J., Seifert, P., & Macke, A. (2022). Radiative closure and cloud effects on the radiation budget based on satellite and shipborne observations during the arctic summer research cruise, ps106. *Atmospheric Chemistry and Physics*, 22(14), 9313–9348. Retrieved from <https://acp.copernicus.org/articles/22/9313/2022/> doi: 10.5194/acp-22-9313-2022
- Bodas-Salcedo, A., Hill, P. G., Furtado, K., Williams, K. D., Field, P. R., Mannes, J. C., ... Kato, S. (2016). Large contribution of supercooled liquid clouds to the solar radiation budget of the southern ocean. *Journal of Climate*, 29(11), 4213 - 4228. Retrieved from <https://journals.ametsoc.org/view/journals/clim/29/11/jcli-d-15-0564.1.xml> doi: 10.1175/JCLI-D-15-0564.1
- Bony, S., Colman, R., Kattsov, V. M., Allan, R. P., Bretherton, C. S., Dufresne, J.-L., ... Webb, M. J. (2006). How well do we understand and evaluate climate change feedback processes? *Journal of Climate*, 19(15), 3445 - 3482. Retrieved from <https://journals.ametsoc.org/view/journals/clim/19/>

- 15/jcli3819.1.xml doi: 10.1175/JCLI3819.1
- Bühl, J., Seifert, P., Myagkov, A., & Ansmann, A. (2016). Measuring ice- and liquid-water properties in mixed-phase cloud layers at the leipzig cloudnet station. *Atmospheric Chemistry and Physics*, 16(16), 10609–10620. Retrieved from <https://acp.copernicus.org/articles/16/10609/2016/> doi: 10.5194/acp-16-10609-2016
- Cesana, G., & Storelvmo, T. (2017). Improving climate projections by understanding how cloud phase affects radiation. *Journal of Geophysical Research: Atmospheres*, 122(8), 4594–4599. Retrieved from <https://agupubs.onlinelibrary.wiley.com/doi/abs/10.1002/2017JD026927> doi: 10.1002/2017JD026927
- Clough, S., Shephard, M., Mlawer, E., Delamere, J., Iacono, M., Cady-Pereira, K., ... Brown, P. (2005). Atmospheric radiative transfer modeling: a summary of the aer codes. *Journal of Quantitative Spectroscopy and Radiative Transfer*, 91(2), 233–244. Retrieved from <https://www.sciencedirect.com/science/article/pii/S0022407304002158> doi: <https://doi.org/10.1016/j.jqsrt.2004.05.058>
- Delanoë, J., Protat, A., Bouniol, D., Heymsfield, A., Bansemer, A., & Brown, P. (2007). The characterization of ice cloud properties from doppler radar measurements. *Journal of Applied Meteorology and Climatology*, 46(10), 1682–1698. Retrieved from <https://journals.ametsoc.org/view/journals/apme/46/10/jam2543.1.xml> doi: 10.1175/JAM2543.1
- Ecmwf forecast user guide. (2018, 05)., 2018. Retrieved from <https://www.ecmwf.int/node/16559> doi: 10.21957/mlcs7h
- Fiddes, S. L., Protat, A., Mallet, M. D., Alexander, S. P., & Woodhouse, M. T. (2022). Southern ocean cloud and shortwave radiation biases in a nudged climate model simulation: does the model ever get it right? *Atmospheric Chemistry and Physics*, 22(22), 14603–14630. Retrieved from <https://acp.copernicus.org/articles/22/14603/2022/> doi: 10.5194/acp-22-14603-2022
- Field, P. R., & Heymsfield, A. J. (2015). Importance of snow to global precipitation. *Geophysical Research Letters*, 42(21), 9512–9520. Retrieved from <https://agupubs.onlinelibrary.wiley.com/doi/abs/10.1002/2015GL065497> doi: <https://doi.org/10.1002/2015GL065497>
- Frisch, A. S., Fairall, C. W., & Snider, J. (1995). Measurement of Stratus Cloud and Drizzle Parameters in ASTEX with a Ka-Band Doppler Radar and a Microwave Radiometer. *J. Atmos. Sci.*, 52(16), 2788–2799.
- Frisch, A. S., Feingold, G., Fairall, C. W., Uttal, T., & Snider, J. B. (1998). On cloud radar and microwave radiometer measurements of stratus cloud liquid water profiles. *Journal of Geophysical Research: Atmospheres*, 103(D18), 23195–23197. Retrieved from <https://agupubs.onlinelibrary.wiley.com/doi/abs/10.1029/98JD01827> doi: <https://doi.org/10.1029/98JD01827>
- Frisch, A. S., Martner, B. E., Djalalova, I., & Poellot, M. R. (2000). Comparison of radar/radiometer retrievals of stratus cloud liquid-water content profiles with in situ measurements by aircraft. *J. Geophys. Res. Atmos.*, 105(D12), 15361–15364. doi: 10.1029/2000jd900128
- Gettelman, A., Bardeen, C. G., McCluskey, C. S., Järvinen, E., Stith, J., Breher-ton, C., ... Wu, W. (2020). Simulating observations of southern ocean clouds and implications for climate. *Journal of Geophysical Research: Atmospheres*, 125(21), e2020JD032619. Retrieved from <https://agupubs.onlinelibrary.wiley.com/doi/abs/10.1029/2020JD032619> (e2020JD032619 10.1029/2020JD032619) doi: <https://doi.org/10.1029/2020JD032619>
- Goyal, R., Sen Gupta, A., Jucker, M., & England, M. H. (2021). Historical and projected changes in the southern hemisphere surface westerlies. *Geophysical Research Letters*, 48(4), e2020GL090849. Retrieved from <https://>

- agupubs.onlinelibrary.wiley.com/doi/abs/10.1029/2020GL090849
(e2020GL090849 2020GL090849) doi: <https://doi.org/10.1029/2020GL090849>
- Gregory, D., & Morris, D. (1996). The sensitivity of climate simulations to the specification of mixed-phase clouds. *Climate Dyn.*, 12, 641–651.
- Griesche, H. J., Seifert, P., Ansmann, A., Baars, H., Barrientos Velasco, C., Bühl, J., ... Macke, A. (2020). Application of the shipborne remote sensing supersite oceanet for profiling of arctic aerosols and clouds during polarstern cruise ps106. *Atmospheric Measurement Techniques*, 13(10), 5335–5358. Retrieved from <https://amt.copernicus.org/articles/13/5335/2020/> doi: 10.5194/amt-13-5335-2020
- Grise, K. M., & Polvani, L. M. (2014a). Southern hemisphere cloud-dynamics biases in cmip5 models and their implications for climate projections. *Journal of Climate*, 27(15), 6074 - 6092. Retrieved from <https://journals.ametsoc.org/view/journals/clim/27/15/jcli-d-14-00113.1.xml> doi: 10.1175/JCLI-D-14-00113.1
- Grise, K. M., & Polvani, L. M. (2014b). Southern hemisphere cloud-dynamics biases in cmip5 models and their implications for climate projections. *Journal of Climate*, 27(15), 6074 - 6092. Retrieved from <https://journals.ametsoc.org/view/journals/clim/27/15/jcli-d-14-00113.1.xml> doi: 10.1175/JCLI-D-14-00113.1
- Grise, K. M., Polvani, L. M., & Fasullo, J. T. (2015). Reexamining the relationship between climate sensitivity and the southern hemisphere radiation budget in cmip models. *Journal of Climate*, 28(23), 9298 - 9312. Retrieved from <https://journals.ametsoc.org/view/journals/clim/28/23/jcli-d-15-0031.1.xml> doi: 10.1175/JCLI-D-15-0031.1
- Heese, B., Flentje, H., Althausen, D., Ansmann, A., & Frey, S. (2010). Ceilometer lidar comparison: backscatter coefficient retrieval and signal-to-noise ratio determination. *Atmospheric Measurement Techniques*, 3(6), 1763–1770. Retrieved from <https://amt.copernicus.org/articles/3/1763/2010/> doi: 10.5194/amt-3-1763-2010
- Hersbach, H., Bell, B., Berrisford, P., Hirahara, S., Horányi, A., Muñoz-Sabater, J., ... Thépaut, J.-N. (2020). The era5 global reanalysis. *Quarterly Journal of the Royal Meteorological Society*, 146(730), 1999–2049. Retrieved from <https://rmets.onlinelibrary.wiley.com/doi/abs/10.1002/qj.3803> doi: <https://doi.org/10.1002/qj.3803>
- Hoffmann, L., & Spang, R. (2022). An assessment of tropopause characteristics of the era5 and era-interim meteorological reanalyses. *Atmospheric Chemistry and Physics*, 22(6), 4019–4046. Retrieved from <https://acp.copernicus.org/articles/22/4019/2022/> doi: 10.5194/acp-22-4019-2022
- Hogan, R. J., Mittermaier, M. P., & Illingworth, A. J. (2006). The retrieval of ice water content from radar reflectivity factor and temperature and its use in evaluating a mesoscale model. *Journal of Applied Meteorology and Climatology*, 45(2), 301 - 317. Retrieved from <https://journals.ametsoc.org/view/journals/apme/45/2/jam2340.1.xml> doi: 10.1175/JAM2340.1
- Hu, Y., Rodier, S., Xu, K.-M., Sun, W., Huang, J., Lin, B., ... Josset, D. (2010). Occurrence, liquid water content and fraction of supercooled water clouds from combined caliop/iir/modis measurements. *J. Geophys. Res.*, 115, D00H34.
- Huang, Y., Siems, S. T., Manton, M. J., Protat, A., & Delanöe, J. (2012). A study on the low-altitude clouds over the southern ocean using the dardar-mask. *J. Geophys. Res.*, 117, D18204.
- Illingworth, A. J., Hogan, R. J., O'Connor, E., Bouniol, D., Brooks, M. E., Delanöe, J., ... Wrench, C. L. (2007). Cloudnet: Continuous evaluation of cloud profiles in seven operational models using ground-based observations. *B. Am. Meteorol. Soc.*, 88(6), 883–898. doi: 10.1175/BAMS-88-6-883

- Kanitz, T., Seifert, P., Ansmann, A., Engelmann, R., Althausen, D., Casiccia, C., & Rohwer, E. G. (2011). Contrasting the impact of aerosols at northern and southern midlatitudes on heterogeneous ice formation. *Geophys. Res. Lett.*, *38*(17). doi: 10.1029/2011GL048532
- Kay, J. E., Wall, C., Yettella, V., Medeiros, B., Hannay, C., Caldwell, P., & Bitz, C. (2016). Global climate impacts of fixing the southern ocean short-wave radiation bias in the community earth system model (cesm). *Journal of Climate*, *29*(12), 4617 - 4636. Retrieved from <https://journals.ametsoc.org/view/journals/clim/29/12/jcli-d-15-0358.1.xml> doi: 10.1175/JCLI-D-15-0358.1
- Komurcu, M., Storelvmo, T., Tan, I., Lohmann, U., Yun, Y., Penner, J. E., ... Takemura, T. (2014). Intercomparison of the cloud water phase among global climate models. *J. Geophys. Res. Atmos.*, *119*(6), 3372–3400. doi: 10.1002/2013jd021119
- Küchler, N., Kneifel, S., Löhnert, U., Kollias, P., Czekala, H., & Rose, T. (2017). A w-band radar–radiometer system for accurate and continuous monitoring of clouds and precipitation. *J. Atmos. Oceanic Technol.*, *34*(11), 2375–2392. doi: 10.1175/jtech-d-17-0019.1
- Li, Z.-X., & Treut, H. L. (1992). Cloud-radiation feedbacks in a general circulation model and their dependence on cloud modeling assumptions. *Climate Dyn.*, *7*, 133–139.
- Mace, G. G., & Protat, A. (2018). Clouds over the southern ocean as observed from the r/v investigator during capricorn. part i: Cloud occurrence and phase partitioning. *Journal of Applied Meteorology and Climatology*, *57*(8), 1783 - 1803. Retrieved from <https://journals.ametsoc.org/view/journals/apme/57/8/jamc-d-17-0194.1.xml> doi: <https://doi.org/10.1175/JAMC-D-17-0194.1>
- Mace, G. G., Protat, A., Humphries, R. S., Alexander, S. P., McRobert, I. M., Ward, J., ... McFarquhar, G. M. (2021). Southern ocean cloud properties derived from capricorn and marcus data. *Journal of Geophysical Research: Atmospheres*, *126*(4), e2020JD033368. Retrieved from <https://agupubs.onlinelibrary.wiley.com/doi/abs/10.1029/2020JD033368> (e2020JD033368 2020JD033368) doi: <https://doi.org/10.1029/2020JD033368>
- McCoy, D. T., Tan, I., Hartmann, D. L., Zelinka, M. D., & Storelvmo, T. (2016). On the relationships among cloud cover, mixed-phase partitioning, and planetary albedo in gcms. *J. Adv. Model. Earth Syst.*, *8*, 650–668.
- McFarquhar, G. M., Bretherton, C. S., Marchand, R., Protat, A., DeMott, P. J., Alexander, S. P., ... McDonald, A. (2021). Observations of clouds, aerosols, precipitation, and surface radiation over the southern ocean: An overview of capricorn, marcus, micre, and socrates. *Bulletin of the American Meteorological Society*, *102*(4), E894 - E928. Retrieved from <https://journals.ametsoc.org/view/journals/bams/102/4/BAMS-D-20-0132.1.xml> doi: 10.1175/BAMS-D-20-0132.1
- Mlawer, E. J., Taubman, S. J., Brown, P. D., Iacono, M. J., & Clough, S. A. (1997). Radiative transfer for inhomogeneous atmospheres: Rrtm, a validated correlated-k model for the longwave. *Journal of Geophysical Research: Atmospheres*, *102*(D14), 16663-16682. Retrieved from <https://agupubs.onlinelibrary.wiley.com/doi/abs/10.1029/97JD00237> doi: 10.1029/97JD00237
- Mobile radiation observatory (MORDOR)*. (2022). <https://www.tropos.de/en/research/projects-infrastructure-technology/technology-at-tropos/remote-sensing/radiation-measurement-station-bsrn>. (Accessed: 2023-02-08)
- Morrison, A. E., Siems, S. T., & Manton, M. J. (2011). A three-year climatology of cloud-top phase over the southern ocean and north pacific. *J. Climate*, *24*, 2405–2418.

- Mülmenstädt, J., Sourdeval, O., Delanoë, J., & Quaas, J. (2015). Frequency of occurrence of rain from liquid-, mixed-, and ice-phase clouds derived from a-train satellite retrievals. *Geophysical Research Letters*, 42(15), 6502-6509. Retrieved from <https://agupubs.onlinelibrary.wiley.com/doi/abs/10.1002/2015GL064604> doi: <https://doi.org/10.1002/2015GL064604>
- Naud, C., Booth, J. F., & Genio, A. D. D. (2014). Evaluation of era-interim and merra cloudiness in the southern ocean. *J. Climate*, 27, 2109-2124.
- Protat, A., Schulz, E., Rikus, L., Sun, Z., Xiao, Y., & Keywood, M. (2017). Ship-borne observations of the radiative effect of southern ocean clouds. *Journal of Geophysical Research: Atmospheres*, 122(1), 318-328. Retrieved from <https://agupubs.onlinelibrary.wiley.com/doi/abs/10.1002/2016JD026061> doi: <https://doi.org/10.1002/2016JD026061>
- Radenz, M., Bühl, J., Seifert, P., Baars, H., Engelmann, R., Barja González, B., ... Ansmann, A. (2021). Hemispheric contrasts in ice formation in stratiform mixed-phase clouds: disentangling the role of aerosol and dynamics with ground-based remote sensing. *Atmospheric Chemistry and Physics*, 21(23), 17969-17994. Retrieved from <https://acp.copernicus.org/articles/21/17969/2021/> doi: 10.5194/acp-21-17969-2021
- Rose, T., Crewell, S., Löhnert, U., & Simmer, C. (2005, may). A network suitable microwave radiometer for operational monitoring of the cloudy atmosphere. *Atmos. Res.*, 75(3), 183-200. doi: 10.1016/j.atmosres.2004.12.005
- Schimmel, W., Kalesse-Los, H., Maahn, M., Vogl, T., Foth, A., Garfias, P. S., & Seifert, P. (2022). Identifying cloud droplets beyond lidar attenuation from vertically pointing cloud radar observations using artificial neural networks. *Atmospheric Measurement Techniques*, 15(18), 5343-5366. Retrieved from <https://amt.copernicus.org/articles/15/5343/2022/> doi: 10.5194/amt-15-5343-2022
- Shupe, M. D., Uttal, T., & Matrosov, S. Y. (2005). Arctic cloud microphysics retrievals from surface-based remote sensors at sheba. *Journal of Applied Meteorology*, 44(10), 1544-1562. Retrieved from <https://doi.org/10.1175/JAM2297.1> doi: 10.1175/JAM2297.1
- Sun, Z., & Shine, K. P. (1994). Studies of the radiative properties of ice and mixed-phase clouds. *Quarterly Journal of the Royal Meteorological Society*, 120(515), 111-137. Retrieved from <https://rmets.onlinelibrary.wiley.com/doi/abs/10.1002/qj.49712051508> doi: <https://doi.org/10.1002/qj.49712051508>
- Tan, I., & Storelvmo, T. (2019). Evidence of strong contributions from mixed-phase clouds to arctic climate change. *Geophysical Research Letters*, 46(5), 2894-2902. Retrieved from <https://agupubs.onlinelibrary.wiley.com/doi/abs/10.1029/2018GL081871> doi: <https://doi.org/10.1029/2018GL081871>
- Tukiainen, S., O'Connor, E., & Korpinen, A. (2020). Cloudnetpy: A python package for processing cloud remote sensing data. *J. Open Source Softw.*, 5(53), 2123. doi: 10.21105/joss.02123
- Turner, D. D., Shupe, M. D., & Zwink, A. B. (2018). Characteristic atmospheric radiative heating rate profiles in arctic clouds as observed at barrow, alaska. *Journal of Applied Meteorology and Climatology*, 57(4), 953 - 968. Retrieved from <https://journals.ametsoc.org/view/journals/apme/57/4/jamc-d-17-0252.1.xml> doi: 10.1175/JAMC-D-17-0252.1
- Wang, T., Fetzer, E. J., Wong, S., Kahn, B. H., & Yue, Q. (2016). Validation of modis cloud mask and multilayer flag using cloudsat-calipso cloud profiles and a cross-reference of their cloud classifications. *Journal of Geophysical Research: Atmospheres*, 121(19), 11,620-11,635. Retrieved from <https://agupubs.onlinelibrary.wiley.com/doi/abs/10.1002/2016JD025239> doi: <https://doi.org/10.1002/2016JD025239>
- Witthuhn, J., Hünerbein, A., Filipitsch, F., Wacker, S., Meilinger, S., & Deneke, H. (2021). Aerosol properties and aerosol-radiation interactions in clear sky

- 628 conditions over germany. *Atmospheric Chemistry and Physics Discussions*,
 629 *2021*, 1–64. Retrieved from [https://acp.copernicus.org/preprints/](https://acp.copernicus.org/preprints/acp-2021-517/)
 630 [acp-2021-517/](https://acp.copernicus.org/preprints/acp-2021-517/) doi: 10.5194/acp-2021-517
- 631 Xi, B., Dong, X., Zheng, X., & Wu, P. (2022). Cloud phase and macrophysical
 632 properties over the southern ocean during the marcus field campaign. *Atmo-*
 633 *spheric Measurement Techniques*, *15*(12), 3761–3777. Retrieved from [https://](https://amt.copernicus.org/articles/15/3761/2022/)
 634 amt.copernicus.org/articles/15/3761/2022/ doi: 10.5194/amt-15-3761
 635 -2022
- 636 Zaremba, T. J., Rauber, R. M., McFarquhar, G. M., Hayman, M., Finlon, J. A.,
 637 & Stechman, D. M. (2020). Phase characterization of cold sector south-
 638 ern ocean cloud tops: Results from socrates. *Journal of Geophysical Re-*
 639 *search: Atmospheres*, *125*(24), e2020JD033673. Retrieved from [https://](https://agupubs.onlinelibrary.wiley.com/doi/abs/10.1029/2020JD033673)
 640 agupubs.onlinelibrary.wiley.com/doi/abs/10.1029/2020JD033673
 641 (e2020JD033673 2020JD033673) doi: <https://doi.org/10.1029/2020JD033673>
- 642 Zhang, D., Wang, Z., & Liu, D. (2010). A global view of midlevel liquid-layer
 643 topped stratiform cloud distribution and phase partition from calipso and
 644 cloudsat measurements. *Journal of Geophysical Research: Atmospheres*,
 645 *115*(D4). Retrieved from [https://agupubs.onlinelibrary.wiley.com/doi/](https://agupubs.onlinelibrary.wiley.com/doi/abs/10.1029/2009JD012143)
 646 [abs/10.1029/2009JD012143](https://agupubs.onlinelibrary.wiley.com/doi/abs/10.1029/2009JD012143) doi: <https://doi.org/10.1029/2009JD012143>

Figure 1.

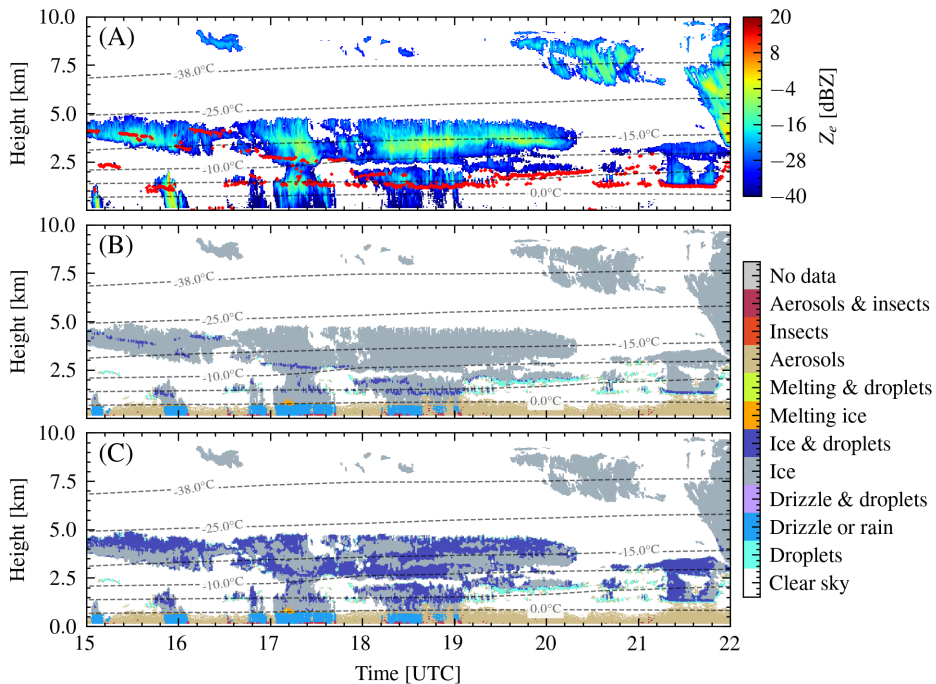


Figure 2.

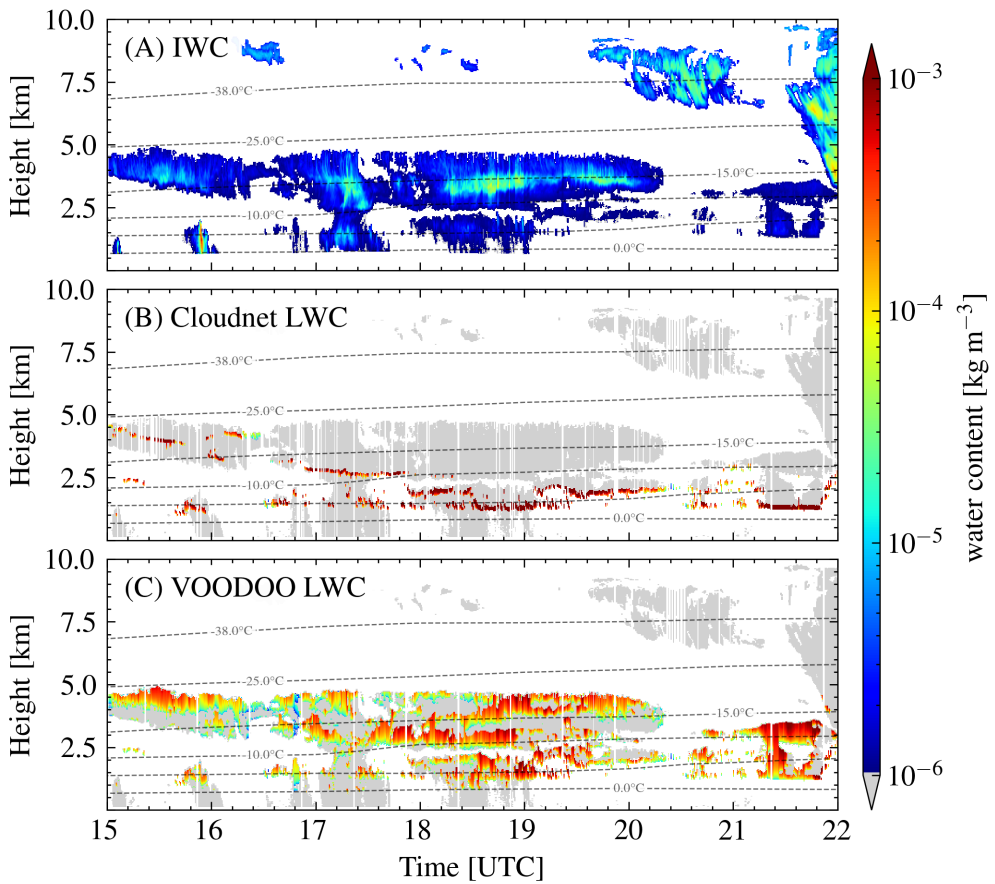


Figure 3.

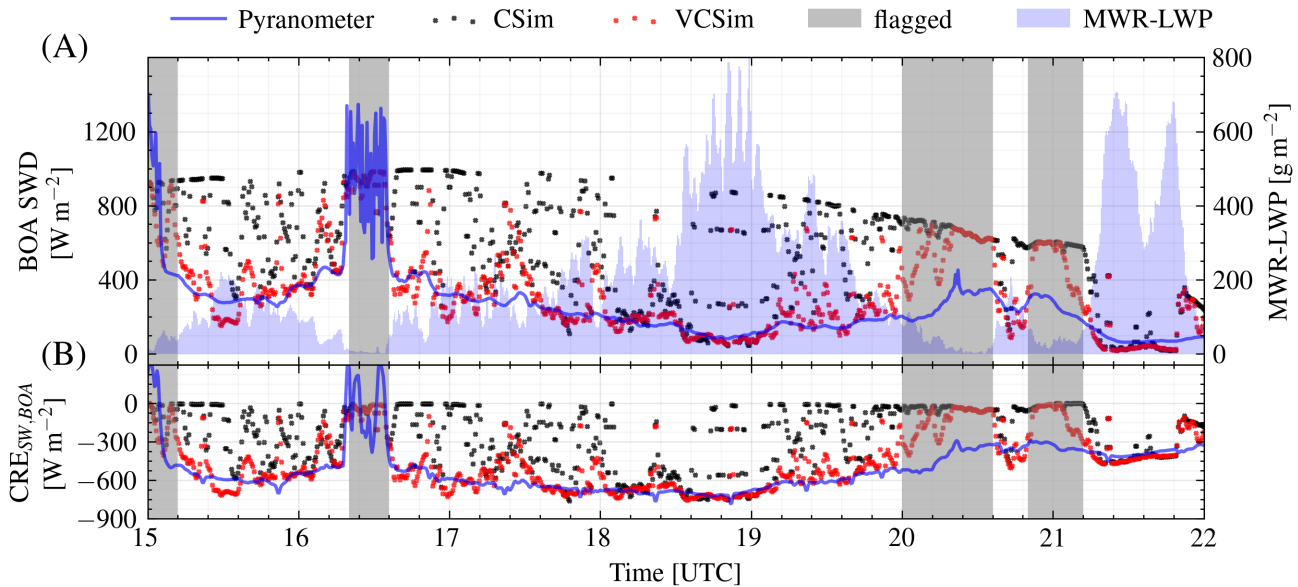


Figure 4.

